Theoretical & Applied Mechanics Letters 11 (2020) 100253

Contents lists available at ScienceDirect

Theoretical & Applied Mechanics Letters

journal homepage: www.elsevier.com/locate/taml

Letter

Bedding plane-embedded augmented virtual internal bonds for fracture propagation simulation in shale

Zihan Liu[a], Zhennan Zhang[a,*], Ahmad Ghassemi[b]

[a] Department of Civil Engineering, Shanghai Jiao Tong University, Shanghai, 200240, China
[b] Mewbourne School of Petroleum and Geological Engineering, The University of Oklahoma, Norman, OK 73091, USA

HIGHLIGHTS

- Bedding plane is embedded into the constitutive model of augmented virtual internal bond.
- The BP-embedded AVIB can represent various Poisson ratio of rock.
- The BP-embedded AVIB can simulate the fracture propagation in transverse isotropic rock.

ARTICLE INFO

Article history:
Received 5 March 2021
Received in revised form 1 April 2021
Accepted 25 April 2021
Available online 30 April 2021

Keywords:
Shale
Bedding plane
Constitutive model
Hydraulic fracture
Augmented virtual internal bond

ABSTRACT

To effectively simulate the fracture propagation in shale, the bedding plane (BP) effect is incorporated into the augmented virtual internal bond (AVIB) constitutive relation through BP tensor. Comparing the BP-embedded AVIB with the theory of transverse isotropy, it is found the approach can represent the anisotropic properties induced by parallel BPs. Through the simulation example, it is found that this method can simulate the stiffness anisotropy of shale and can represent the effect of BPs on hydraulic fracture propagation direction. Compared with the BP-embedded VIB, this method can account for the various Poisson's ratio. It provides a feasible approach to simulate the fracture propagation in shale.

The rock with parallel bedding planes (BP) is quite popular in practical engineering. These BPs make the rock transverse isotropic and significantly affect the fracture propagation in such rock. So far there are generally two approaches to consider the BP, namely the discrete and the continuum approach. In the discrete approach, the BP is individually considered in the numerical model. For instance, Zhao et al. [1] modeled BP by contact interfaces. Li and Zhang [2] considered the BP effect in cohesive finite element method by assigning the interfaces parallel to BP with different parameters. In the discrete approach, the BP can be individuality accounted through a straightforward manner. However, it is hard to handle the massive BPs by the discrete approach since it usually involves a lot of degrees of freedom.

In the continuum approach, the BP is accounted through the constitutive relation. For instance, Li et al. [3] coupled a cylindrical microplane system with the classical spherical microplane one [4] together to reflect the transverse isotropy induced by BPs. This method is efficient to represent the high degree of anisotropy of shale. Nguyen and Le [5] developed a microstructure tensor-based method to formulate the anisotropic rock. Compared with the discrete approach, the continuum one has great advantage in reducing degree of freedom. Thus, it is easy to handle the massive BPs. But the continuum method has some limitations in fracture simulation in that it needs a separate fracture criterion to predict fracture propagation. It is hard to find a suitable fracture criterion for the anisotropic rock.

Recently, Zhang et al. [6] proposed a new approach to model the shale with consideration of BPs in the virtual internal bond (VIB) model [7]. In this method, a BP tensor is defined to quantify the BP distribution. To account for the BP effect, the bond distribution density is associated with the BP tensor. However, in

* Corresponding author.
E-mail address: zhennanzhang@sjtu.edu.cn.

http://dx.doi.org/10.1016/j.taml.2021.100253

this work, the Poisson's ratio is fixed. In this letter, we incorporate the BP tensor into the augmented virtual internal bond (AVIB) model [8] in order to improve model accuracy of VIB. The BP-embedded AVIB can handle the massive BPs through constitutive relation and can avoid the separate fracture criterion in fracture simulation.

The AVIB [8] is a micro-macro constitutive model that stems from the VIB [7]. The representative element volume (REV) of VIB consists of bond network on the micro scale (Fig. 1a). In AVIB, the Xu-Needleman potential [9] is adopted to quantify the strain energy of a bond, which reads

$$U(\Delta_n,\Delta_t)=\phi_n-\phi_n\exp\left(-\frac{\Delta_n}{\delta_n}\right)\left[1+\frac{\Delta_n}{\delta_n}\right]\left[1-q+q\exp\left(-\frac{\Delta_t^2}{\delta_t^2}\right)\right], \tag{1}$$

where Δ_n,Δ_t are the normal and tangent deformation of a bond, respectively; δ_n and δ_t are the characteristic lengths for the normal and tangential deformation, $\delta_n=\delta_t=\tilde{\varepsilon}_t l_0$; $\tilde{\varepsilon}_t$ is the strain of bond at the peak uniaxial tensile force, usually taking $\tilde{\varepsilon}_t\approx\varepsilon_t$ with ε_t being the strain value at the peak stress of the uniaxial tension stress-strain curve of material; ϕ_n stands for the energy related to the normal bond deformation and q the energy ratio of the normal bond deformation to the tangent one. Their relationship with the macro constants is

$$\phi_n=\frac{V\delta_n^2}{l_0^2}\cdot\frac{3E}{4\pi(1-2\nu)},\qquad q=\frac{\delta_t^2}{\delta_n^2}\cdot\frac{(1-4\nu)}{2(1+\nu)}, \tag{2}$$

where E is the Young's modulus, ν the Poisson's ratio, l_0 the undeformed bond length and V the volume of REV.

According to the Cauchy-Born rule [10], the bond deformations (shown in Fig. 1b) are associated with the macro strain tensor by

$$\Delta_n=\xi^{\mathrm{T}}\varepsilon\xi l_0,\qquad \Delta_t^2=\left[\xi^{\mathrm{T}}\varepsilon^{\mathrm{T}}\varepsilon\xi-\left(\xi^{\mathrm{T}}\varepsilon\xi\right)^2\right]l_0^2, \tag{3}$$

where ε is the strain tensor of the REV and ξ the bond orientation vector, $\xi=\left[\sin\theta\cos\varphi,\sin\theta\sin\varphi,\cos\theta\right]^{\mathrm{T}}$ in the spherical coordinate system (Fig. 1b); the superscript '$_T$' means the transpose.

With Eq.(1–3), the stress tensor of AVIB is derived as

$$\sigma_{ij}=\frac{1}{V}\cdot\frac{\partial}{\partial\varepsilon_{ij}}\int_0^{2\pi}\int_0^{\pi}U(\Delta_n,\Delta_t)\cdot D(\theta,\varphi)\cdot\sin\theta\,\mathrm{d}\theta\mathrm{d}\phi, \tag{4}$$

and the tangent modulus tensor is

$$K_{ijkl}=\frac{1}{V}\cdot\frac{\partial^2}{\partial\varepsilon_{ij}\partial\varepsilon_{kl}}\int_0^{2\pi}\int_0^{\pi}U(\Delta_n,\Delta_t)\cdot D(\theta,\varphi)\cdot\sin\theta\,\mathrm{d}\theta\mathrm{d}\phi, \tag{5}$$

where $D(\theta,\varphi)$ is the bond distribution density in terms of the spherical coordinates θ and φ.

For a shale which contains numerous BPs, shown in Fig. 2, Zhang et al. [6] have established the BP tensor to quantify BP. That is

$$\Omega=\mathbf{Q}^{\mathrm{T}}\bar{\Omega}\mathbf{Q}, \tag{6}$$

where $\bar{\Omega}$ is the local BP tensor in the local coordinate of BP, $\bar{\Omega}=\mathrm{Diag}(0,0,\omega)$. ω is a parameter varying from 0 to 1, which reflects the weakening degree of shale stiffness in the normal bedding direction. $\mathbf{Q}$ is the global-to-local coordinate

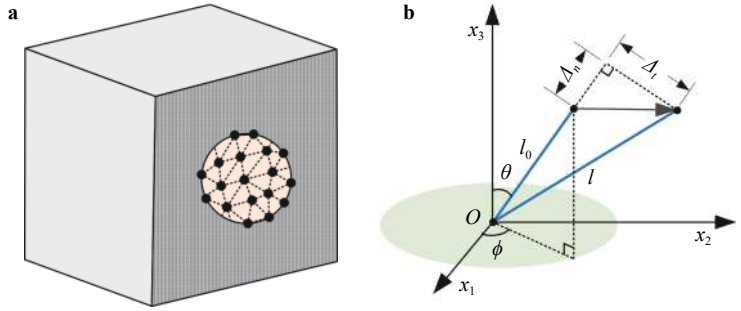

Fig. 1. AVIB model **a** representative element volume of AVIB; **b** a bond in the spherical coordinate system.

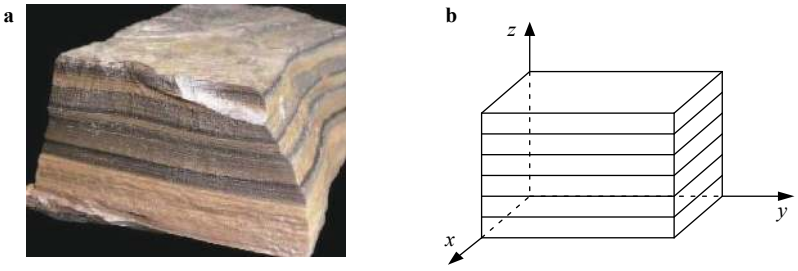

Fig. 2. Bedding planes of shale **a** shale sample; **b** BPs in local coordinate system.

transformation matrix

$$\mathbf{Q}=\begin{bmatrix}\cos H & -\sin H & 0\\ \sin H\cos R & \cos H\cos R & -\sin R\\ \sin H\sin R & \cos H\sin R & \cos R\end{bmatrix}, \tag{7}$$

where the H being the azimuth and R the dip angle of BP.

In Ref. [6], the bond distribution density in the direction ξ is associated with the BP tensor through

$$D(\xi)=1-\lambda\omega(\xi)=1-\lambda\xi^{\mathrm{T}}\Omega\xi. \tag{8}$$

In this letter, the bond distribution density of AVIB is quantified by the same manner. Thus, the constitutive relation of BP-embedded AVIB is

$$\sigma_{ij}=\frac{\partial}{\partial\varepsilon_{ij}}\left[\frac{1}{V}\int_0^{2\pi}\int_0^{\pi/2}U(\Delta_n,\Delta_t)\left(1-\lambda\xi^{\mathrm{T}}\Omega\xi\right)\sin\theta\mathrm{d}\theta\mathrm{d}\varphi\right], \tag{9}$$

where λ is a coefficient to be calibrated in the following context.

To what degree that the BP-embedded AVIB can represent a transverse isotropic solid (TIS) is a key point. It will be discussed in the following.

In the linear elasticity theory, the elastic matrix $\mathbf{C}$ of TIS is defined through $[\sigma_{11},\sigma_{22},\sigma_{33},\sigma_{12},\sigma_{23},\sigma_{31}]^{\mathrm{T}}=.\ \mathbf{C}\left[\varepsilon_{11},\varepsilon_{22},\varepsilon_{33},\gamma_{12},\gamma_{23},\gamma_{31}\right]^{\mathrm{T}}$The elastic matrix is expressed as

$$\mathbf{C}=\begin{bmatrix}C_1 & C_2 & C_3 & 0 & 0 & 0\\ & C_1 & C_3 & 0 & 0 & 0\\ & & C_4 & 0 & 0 & 0\\ & \text{Symmetric} & & (C_1-C_2)/2 & 0 & 0\\ & & & & C_5 & 0\\ & & & & & C_5\end{bmatrix}, \tag{10}$$

whose components are

$$C_1=\frac{\left(1-\alpha\beta^2\nu_p^2\right)E_p}{\left(1+\nu_p\right)\left(1-\nu_p-2\alpha\beta^2\nu_p^2\right)},\ C_2=\frac{\nu_p\left(1+\alpha\beta^2\nu_p\right)E_p}{\left(1+\nu_p\right)\left(1-\nu_p-2\alpha\beta^2\nu_p^2\right)},$$
$$C_3=\frac{\alpha\beta\nu_pE_p}{1-\nu_p-2\alpha\beta^2\nu_p^2},\ C_4=\frac{\alpha\left(1-\nu_p\right)E_p}{1-\nu_p-2\alpha\beta^2\nu_p^2},\ C_5=\frac{\kappa E_p}{2\left(1+\nu_p\right)}. \tag{11}$$

In these components, $\alpha=E_z/E_p$, $\beta=\nu_{pz}/\nu_p$ and $\kappa=G_{zp}/G_p$, where E_{p} and ν_{p} are the Young's modulus and Poisson's ratio in the x-y symmetry plane, respectively; E_{pz} and ν_{pz} are those in the z-direction, respectively; G_{zp} is the shear modulus in the z-direction. For the TIS solid, the relationship $\nu_{zp}/E_z=\nu_{pz}/E_p$ holds, so $\nu_{zp}=\alpha\beta\nu_p$. Therefore, the TIS solid has five independent parameters, i.e., $\{E_p,\nu_p,\alpha,\beta,\kappa\}$.

According to Eq. (5), the tangent modulus of AVIB can be derived as $K_{ijkl}=\partial\sigma_{ij}/\partial\varepsilon_{kl}$. At the initial state, i.e., $\varepsilon=0$, the tangent modulus is

$$K_{ijkl}=\int_0^{2\pi}\int_0^{\pi}\left[(A-B)\xi_i\xi_j\xi_k\xi_l+B\delta_{ik}\xi_j\xi_l\right]\left(1-\lambda\xi^{\mathrm{T}}\Omega\xi\right)\sin\theta\mathrm{d}\theta\mathrm{d}\phi, \tag{12}$$

where

$$A=\frac{3E}{4\pi\ (1-2\nu)},$$
$$B=\frac{3E(1-4\nu)}{4\pi\ (1+\nu)(1-2\nu)}. \tag{13}$$

By integrating Eq. (12), the elastic matrix $\mathbf{D}$ of AVIB is obtained

$$\mathbf{D}=\begin{bmatrix}D_1 & D_2 & D_3 & 0 & 0 & 0\\ & D_1 & D_3 & 0 & 0 & 0\\ & & D_4 & 0 & 0 & 0\\ & \text{Symmetric} & & (D_1-D_2)/2 & 0 & 0\\ & & & & D_5 & 0\\ & & & & & D_5\end{bmatrix}, \tag{14}$$

whose components are

$$D_1=\frac{4\pi\ (21A+14B-3A\lambda\omega-4B\lambda\omega)}{105V},\ D_2=\frac{4\pi\ (B-A)\ (\lambda\omega-7)}{105V},$$
$$D_3=\frac{4\pi\ (B-A)\ (3\lambda\omega-7)}{105V},\ D_4=\frac{4\pi\ (21A+14B-15A\lambda\omega-6B\lambda\omega)}{105V},$$
$$D_5=\frac{2\pi\ (14A+21B-6A\lambda\omega-15B\lambda\omega)}{105V}. \tag{15}$$

Due to the effect of BP, the weakening degree in the normal direction of BP can be characterized by D_4/D_1. In the limit case of $\omega=0$, $D_4/D_1=1$ holds while in the limit case of $\omega=1$, $D_4/D_1=0$ holds. Therefore, the coefficient λ is derived as

$$\lambda=\frac{35\,(1-\upsilon)}{3\,(7-3\,\upsilon)}. \tag{16}$$

In Eq. (16), when $\upsilon=0.25$, AVIB is reduced to VIB. Correspondingly, $\lambda|_{\upsilon=0.25}=1.4$, which is consistent with that of Ref. [6].

Through the comparison between the two elastic matric, i.e, Eq. (10) and Eq. (14), we can recognize how the AVIB can represent a TIS. At first, the most important feature of the TIS matrix lies in its structure, i.e. $\bar{C}_{11}=\bar{C}_{22},\bar{C}_{13}=\bar{C}_{23},\bar{C}_{44}=\left(\bar{C}_{11}-\bar{C}_{12}\right)/2$, $\bar{C}_{55}=\bar{C}_{66}$. From Eq. (14), it is seen that the AVIB possesses the same structural feature.

Next, the diagonal components will be compared. According to the physical meaning of α and ω, we have the following relationship

$$\alpha=1-\omega. \tag{17}$$

The stiffness deterioration in the normal direction of BP in

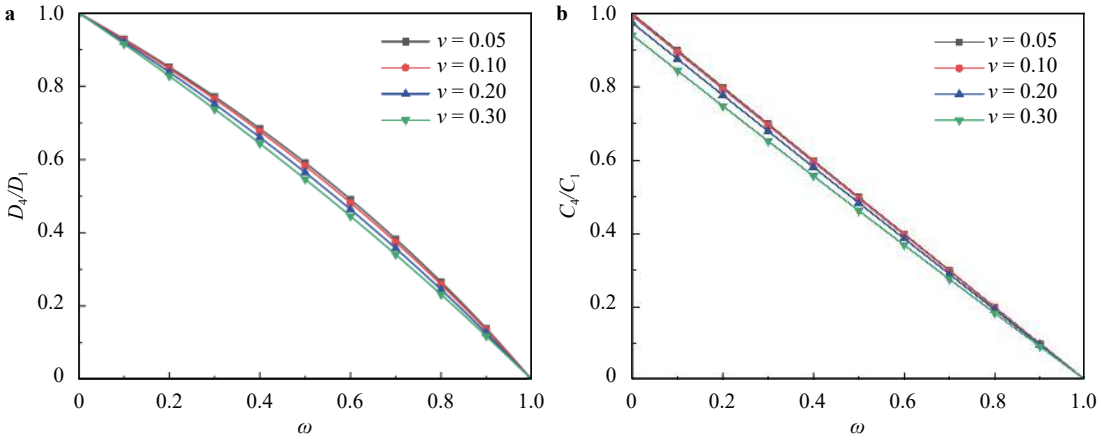

Fig. 3. Stiffness deterioration in the normal direction of BP **a** AVIB; **b** TIS (β =1.0).

AVIB can be expressed by

$$\frac{D_4}{D_1} = \frac{(9\nu - 21)(1-\omega)}{9\nu + 7\omega - 13\nu\omega - 21} \tag{18}$$

while that in TIS is

$$\frac{C_4}{C_1} = \frac{(1-\omega)\left(1-\nu^2\right)}{\beta^2(1-\omega)\nu^2 - 1}. \tag{19}$$

According to Eqs. (18) and (19), the stiffness deterioration is shown in Fig. 3. It is seen that although Eq. (18) is quite different from Eq. (19) in form, they almost linearly decreases from 1 to 0 with ω increasing. That is, the AVIB and TIS present the same trend.

Let D_{i0} and C_{i0} denote the initial value of D_i and C_i corresponding to $\omega = 0$. The influence of BP on the stiffness in orthogonal direction, i.e.,D_1/D_{10} and C_1/C_{10}, is shown in Fig. 4. It is found that the influence of BP on the orthogonal stiffness in AVIB is close to TIS.

In TIS, κ is the ratio of shear modulus in the z-direction to the x-y symmetry plane, which reflects the deterioration degree of shear modulus with BP. Analogous, in AVIB, κ is defined as $\kappa = D_5/G_{iso}$, where G_{iso} denotes the shear modulus of isotropic solid, i.e., $G_{iso} = E/[2(1+\nu)]$. Figure 5 shows the variation of κ with ω. It is seen that κ decreases from 1.0 to about 0.52 with ω increasing from 0 to 0.5. Hou et al. [11] reported that the κ is about 0.58, which falls into the deterioration scope shown in Fig. 5.

The D_2, C_2 and D_3, C_3 variation with BP are shown in Fig. 6. It is seen that the deterioration degrees of off-diagonal components in AVIB and TIS are close.

TIS theory has five independent parameters, i.e.$\{E, \upsilon, \omega, \beta, \kappa\}$, while AVIB has three, i.e,$\{E, \upsilon, \omega\}$. So, AVIB is simpler than the TIS theory although AVIB is not as accurate as TIS in shale description. Compared with the VIB [6], AVIB can account for the Poisson's ratio. Therefore, it is more accurate than VIB.

In order to examine whether the BP-embedded AVIB can reflect the shale anisotropy induced by BPs, the following simulation examples are conducted. The simulation object is a cubic body with inclined BPs. The simulation parameters are as follows: $\omega = 0.5$, $\rho = 2{,}400$ kg/m^3, $E = 40.0$ GPa, $\varepsilon_t = 0.2 \times 10^{-3}$.

The comparison between the simulated and the experimental results [12, 13] is shown in Fig. 7. It is seen that the simulation results are in agreement with the tested ones. So, the present model can capture the anisotropy of shale induced by BPs.

To examine how the BPs impact the hydraulic fracture, the following cases are simulated. Fig. 8 shows the simulation ob-

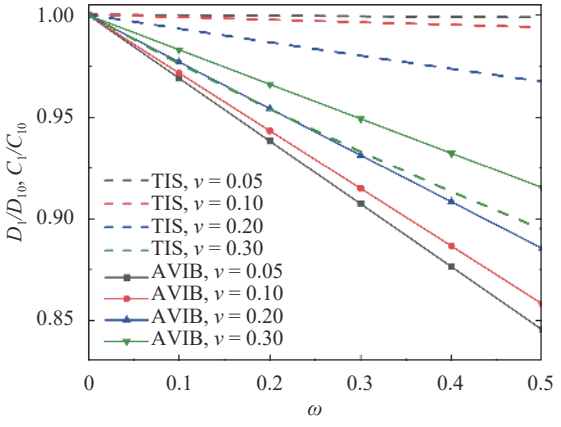

Fig. 4. Influence of BP on the orthogonal stiffness.

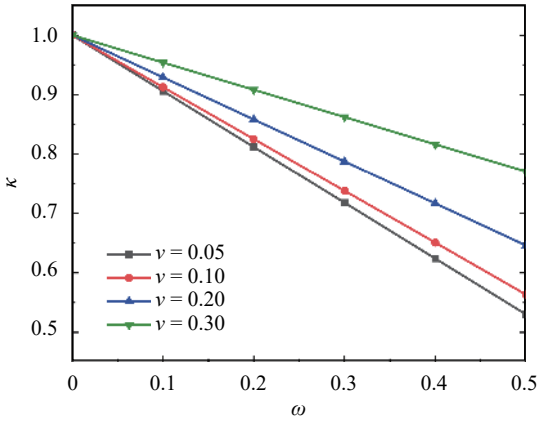

Fig. 5. Influence of BP on shear modulus.

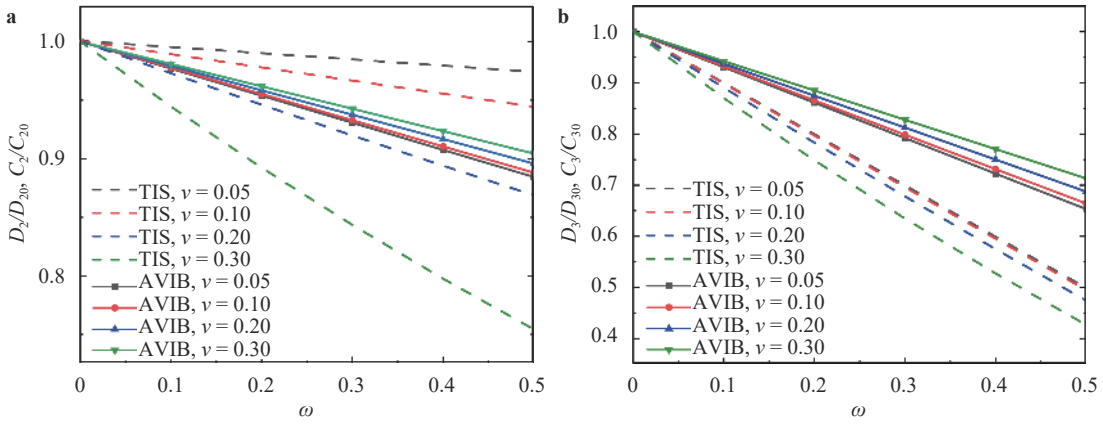

Fig. 6. Off-diagonal element variation with BP **a** D_2/D_{20} and C_2/C_{20}; **b** D_3/D_{30} and C_3/C_{30}.

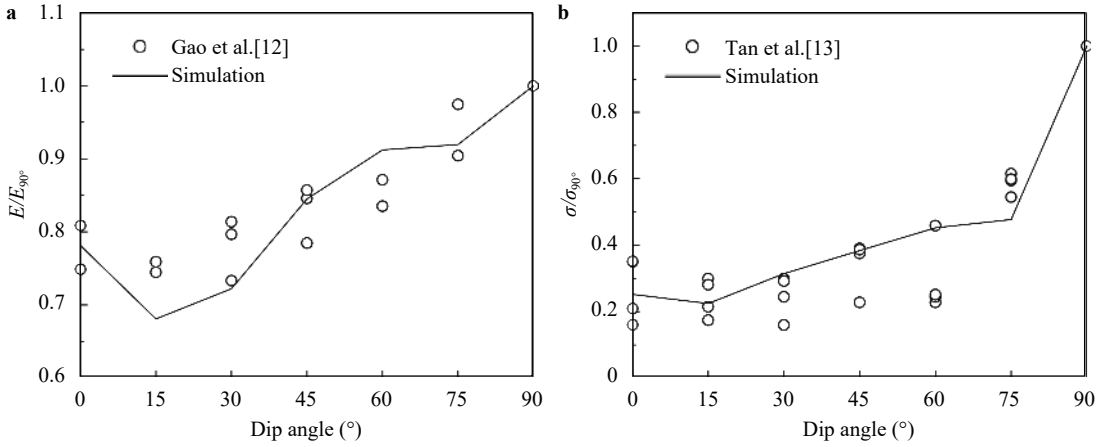

Fig. 7. Comparison between the simulated and experimental results **a** the simulated and the tested stiffness reported in Ref. [12]; **b** the simulated and tested tensile strength reported in Ref.[13].

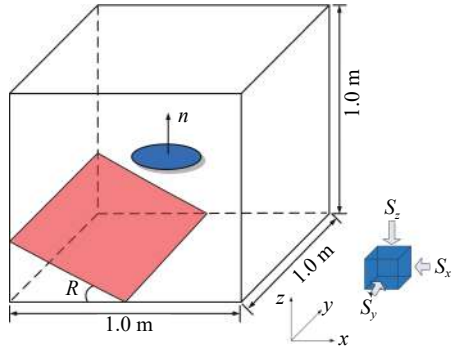

Fig. 8. Simulation object of hydraulic fracture (The red plane represents a bedding plane in the rock).

ject, a cubic body with a preset penny-shaped crack. The size of the simulation object is 1.0 m × 1.0 m × 1.0 m while the radius of the preset crack is 0.2 m. We set the strike of BP aligning with y-axis and the dip angle R. The principal BP value is ω = 0.5. The simulation is conducted in three cases. In Case-1, there is no BP as the reference case. In Case-2 and Case-3, the dip angle of BP is respectively 30 and 60 degrees. To simulate the fracture propagation, the 3D-EPM [14] is employed here. The simulation parameters are: ρ = 2,400 kg/m^3, E = 40.0 GPa and ν = 0.25; flux = 0.15×10^{-6} m^3/s and μ = 0.05 Pa·s. The fluid is injected into the preset crack at a constant flux. In addition, to exclude the impact of in-situ stress, the isotropic in-situ stress are set, which are $S_x = S_y = S_z$ = 5 MPa.

The simulation results of the reference case are shown in Fig. 9a. It is seen that the hydraulic fracture propagates in the horizontal direction, which is reasonable in the isotropic in-situ stresses condition with no BPs. When we set BP at dip angle of 30°, as illustrated in Fig. 9b, the hydraulic fracture no longer propagates along the horizontal direction, instead, approaching to the bedding direction. As the BP angle further increased to 60°, shown in Fig. 9c, the hydraulic crack deflects upward more obviously. These suggest that the BP has significant impact on the hydraulic fracture growth direction. Such influence agrees with the observation in the experiment reported in [15]. Comparing the simulated wellbore pressures in the three cases (Fig. 10), it is found that the peak wellbore pressure with BP is much lower than that without BP. This is due to the weakening effect of BPs.

The bedding plane effect is incorporated into the AVIB through the bedding tensor. By comparison between the BP-em-

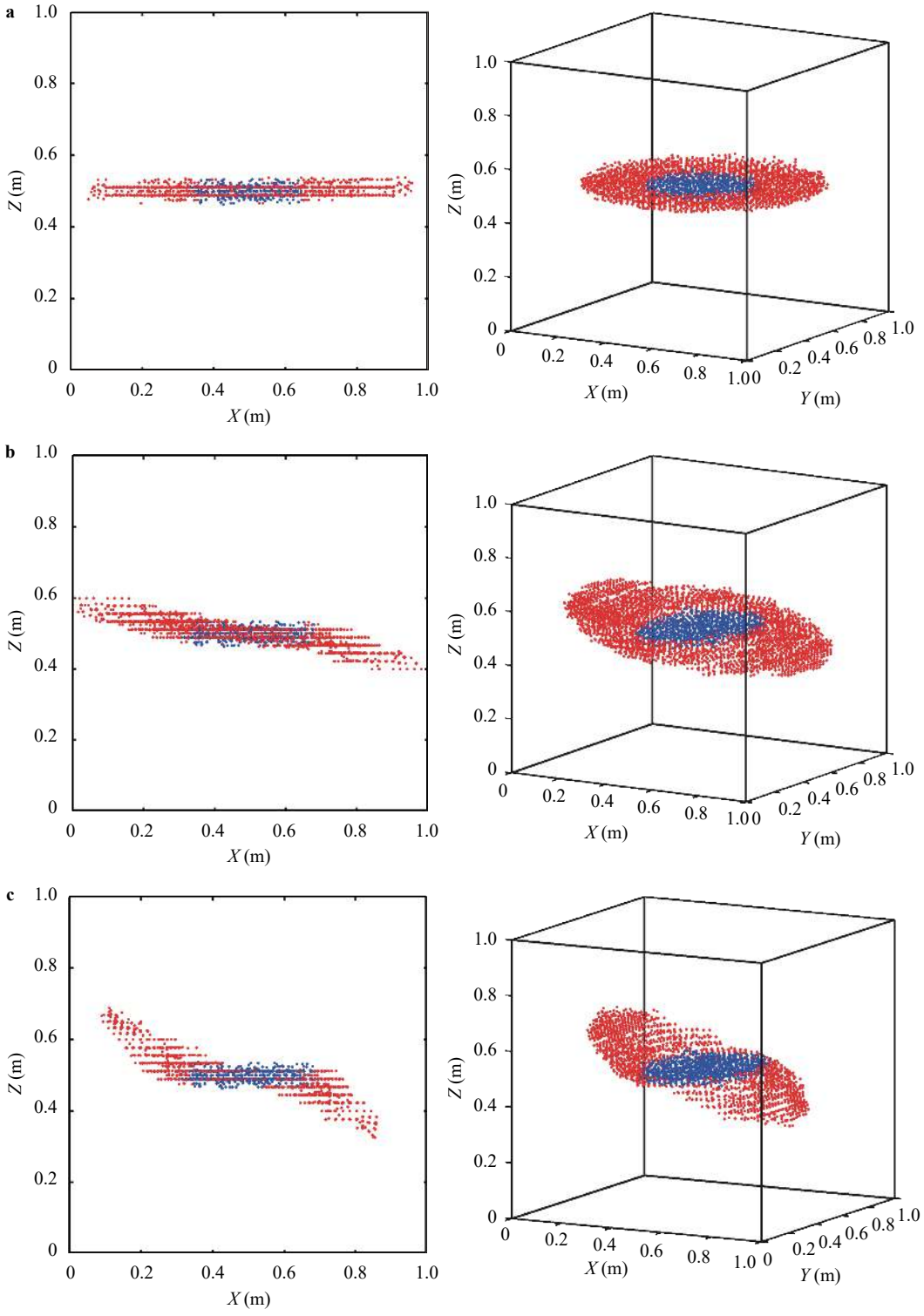

Fig. 9. Simulation results of hydraulic fracture. **a** Case-1; **b** Case-2; **c** Case-3.

bedded AVIB and the transverse isotropic theory, it suggests that such AVIB model can capture the transverse isotropy in theory. The simulation results suggest that this method can simulate the anisotropy of shale induced by BP and it can represent the effect of BP on hydraulic fracture propagation direction in shale. This study provides a new constitutive relation approach to simulate fracture propagation in rock with consideration of bedding plane effect.

Acknowledge

This work is supported by the National Natural Science

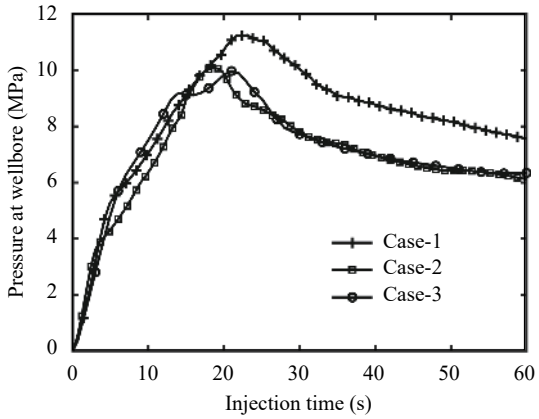

Fig. 10. Simulated wellbore pressure versus time.

Foundation of China (Grant No. 11772190), which is gratefully acknowledged.

References

[1] J. Zhao, Y. Zhang, P.G. Ranjith, Numerical simulation of blasting-induced fracture expansion in coal masses, International Journal of Rock Mechanics and Mining Sciences 100 (2017) 28–39.

[2] C. Li, Z. Zhang, Modeling shale with consideration of bedding planes by cohesive finite element method, Theoretical and Applied Mechanics Letters 9 (2019) 397–402.

[3] C. Li, F.C. Caner, V.T. Chau, et al., Spherocylindrical microplane constitutive model for shale and other anisotropic rocks, Journal of the Mechanics and Physics of Solids 103 (2017) 155–178.

[4] Z.P. Bažant, B.H. Oh, Microplane model for progressive fracture of concrete and rock, Journal of Engineering Mechanics 111 (1985) 559–582.

[5] T.S. Nguyen, A.D. Le, Development of a constitutive model for a bedded argillaceous rock from triaxial and true triaxial tests, Canadian Geotechnical Journal 52 (2015) 1072–1086.

[6] Z. Zhang, Z. Liu, A. Ghassemi, Constitutive modeling of shale with consideration of bedding plane effect by virtual internal bonds, (Submitted, under review 2021)

[7] H. Gao, P. Klein, Numerical simulation of crack growth in an isotropic solid with randomized internal cohesive bonds, Journal of the Mechanics and Physics of Solids 46 (1998) 187–218.

[8] Z. Zhang, H. Gao, Simulating fracture propagation in rock and concrete by an augmented virtual internal bond method, International Journal for Numerical and Analytical Methods in Geomechanics 36 (2012) 459–482.

[9] X.P. Xu, A. Needleman, Numerical simulations of fast crack growth in brittle solids, Journal of the Mechanics and Physics of Solids 42 (1994) 111–132.

[10] E.B. Tadmor, M. Ortiz, R. Phillips, Quasicontinuum analysis of defects in solids, Philosophical Magazine A 73 (1996) 1529–1563.

[11] P. Hou, F. Gao, Z. Zhang, B et al., Mechanical property and bedding inclination effect on gas fracturing of black shale, Chinese Journal of Rock Mechanics and Engineering 35 (2016) 670–681. (in Chinese)

[12] C. Gao, L.Z. Xie, H.P. Xie, et al., Estimation of the equivalent elastic modulus in shale formation: theoretical model and experiment, Journal of Petroleum Science and Engineering 151 (2017) 468–479.

[13] X. Tan, H. Konietzky, T. Frühwirt, et al., Brazilian tests on transversely isotropic rocks: laboratory testing and numerical simulations, Rock Mechanics and Rock Engineering 48 (2015) 1341–1351.

[14] Z. Zhang, D. Wang, X. Ge, et al., Three-dimensional element partition method for fracture simulation, International Journal of Geomechanics 16 (2016) 4015074.

[15] C. Lin, J. He, X. Li, et al., An experimental investigation into the effects of the anisotropy of shale on hydraulic fracture propagation, Rock Mechanics and Rock Engineering 50 (2017) 543–554.